The sidewall-localized mode in a resonant precessing cylinder

Dali Kong, Xinhao Liao, and Keke Zhang

Citation: Physics of Fluids **26**, 051703 (2014); doi: 10.1063/1.4876924
View online: http://dx.doi.org/10.1063/1.4876924
View Table of Contents: http://scitation.aip.org/content/aip/journal/pof2/26/5?ver=pdfcov
Published by the AIP Publishing

PHYSICS OF FLUIDS **26**, 051703 (2014)

The sidewall-localized mode in a resonant precessing cylinder

Dali Kong,[1] Xinhao Liao,[2] and Keke Zhang[1,a)]
[1]*Department of Mathematical Sciences, University of Exeter, Exeter EX4 4QE, United Kingdom*
[2]*Key Laboratory of Planetary Sciences, Shanghai Astronomical Observatory, Chinese Academy of Sciences, Shanghai 200030, China*

(Received 7 February 2014; accepted 28 April 2014; published online 15 May 2014)

We investigate, via direct numerical simulation using a finite-element method, the precessionally driven flow of a homogeneous fluid confined in a fluid-filled circular cylinder that rotates rapidly about its symmetry axis and precesses about a different axis that is fixed in space. Our numerical simulation, after validating with the asymptotic analytical solution for a weakly precessing cylinder and with the constructed exact solution for the strongly nonlinear problem, focuses on the strongly precessing flow at asymptotically small Ekman numbers. An unusual form of the resonant precessing flow is found when the precessing rate is sufficiently large and the corresponding nonlinearity is sufficiently strong. The nonlinear precessing flow is marked by a sidewall-localized non-axisymmetric traveling wave and a wall-localized axisymmetric shear together with an overwhelmingly dominant interior rigid-body rotation whose direction and magnitude substantially reduce the angular momentum of the rotating fluid system. © *2014 AIP Publishing LLC*. [http://dx.doi.org/10.1063/1.4876924]

As a consequence of the controlling influence of rotational effects, fluid motion in rapidly rotating systems often exhibits unusual, intricate behaviors. For example, the convective flow confined in a fluid-filled circular cylinder that rotates rapidly about its symmetry axis and is heated from below concentrates only in the vicinity of its sidewall, which is usually referred to as the sidewall-localized convection.[1–4] The sidewall-localized convection in a rotating cylinder represents a linear phenomenon. When the cylinder rotates rapidly, its fundamental dynamics is intuitively illustrated by the Proudman-Taylor theorem which states that infinitesimal steady motions in a rotating inviscid fluid are two dimensional with respect to the direction of rotation. In other words, the effect of rotation strongly constrains and stabilizes the rotating system. For fluids with moderate Prandtl numbers, the only way of breaking the rotational constraint is to invoke large viscosity with small-scale convection cells. The vicinity of the sidewall in a cylinder offers a special region where the traveling convective wave can be trapped and where convective instability maximizes the viscous effect required to break the rotational constraint and minimizes the vertical temperature gradient needed to initiate convection. Nonlinear effects do not play a role in producing the sidewall-localized convection in rotating cylinders.

The sidewall-localized precessing flow in a circular cylinder reported in this letter represents a strongly nonlinear phenomenon. The problem of precessing flow in circular cylinders, owning to its connection with the dynamics of spinning spacecraft with fluid payloads as well as planetary precession, has been extensively studied.[5–10] It is concerned with a homogeneous fluid of viscosity ν confined in a fluid-filled cylinder of height d and radius Γd that rotates rapidly with angular velocity $\mathbf{\Omega}_0$ about its symmetry axis and precesses with angular velocity $\mathbf{\Omega}_p$ about a different axis that is fixed in space. Three key dimensionless parameters characterize the problem: the Ekman number $Ek = \nu/|\mathbf{\Omega}_0|d^2$ providing the measure of relative importance between the typical viscous

a)Electronic mail: kzhang@ex.ac.uk

force and the Coriolis force, the Poincaré number $Po = |\mathbf{\Omega}_p|/|\mathbf{\Omega}_0|$ quantifying the strength of the precessional forcing and the radius-height aspect ratio Γ controlling the condition of resonance. It is known that the solution of the weakly precessing flow at resonance for $0 < Po/\sqrt{Ek} < \mathrm{O}(1)$ and $0 < Ek \ll 1$ comprises a single dominant inertial mode and a weak geostrophic flow[7,10] and that the strongest resonance takes place at the aspect ratio $\Gamma = 0.502559$ where the frequency of the Poincaré force is the exactly same as that of the primary inertial mode which has the simplest spatial structure.[5] At resonances, the amplitude $|\mathbf{u}|$ of the weakly precessing flow obeys the asymptotic scaling $|\mathbf{u}| = \mathrm{O}(Po/\sqrt{Ek})$ at $0 < Ek \ll 1$.

In this study, we shall reveal an unusual form of the strongly precessing flow when $Po/\sqrt{Ek} = \mathrm{O}(10)$ and $0 < Ek \ll 1$ which is profoundly different from the weakly precessing flow. It is found that the strongly nonlinear flow is quasi-steady and consists of the three major components: a sidewall-localized non-axisymmetric traveling wave, a wall-localized axisymmetric shear, and a dominant interior rigid-body rotation whose direction and magnitude are such that the angular momentum of the rotating fluid system is substantially reduced. Although the sidewall-localized precessing flow is also a consequence of controlling rotational effects at $0 < Ek \ll 1$, the key mechanism of its formation differs fundamentally from that of the sidewall-localized convection.

Consider a homogeneous fluid of viscosity ν and density ρ_0 confined in a fluid-filled circular cylinder of radius Γd and height d. The cylinder rotates rapidly with angular velocity $\mathbf{\Omega}_0 = \hat{\mathbf{z}}\mathbf{\Omega}_0$ about its symmetry axis $\hat{\mathbf{z}}$ and precesses with angular velocity $\mathbf{\Omega}_p$ that is fixed in space and at an angle α, $0 < \alpha \le \pi/2$, with $\hat{\mathbf{z}}$. We shall adopt cylindrical polar coordinates (s, ϕ, z) with $s = 0$ representing the symmetry axis, $z = 0$ at the bottom surface and the corresponding unit vectors $(\hat{\mathbf{s}}, \hat{\boldsymbol{\phi}}, \hat{\mathbf{z}})$. On employing the height d as the length scale, Ω_0^{-1} as the unit of time, and $\rho_0 d^2\Omega_0^2$ as the unit of pressure, we obtain the dimensionless governing equations in the mantle frame of reference:

$$\frac{\partial \mathbf{u}}{\partial t} + \mathbf{u}\cdot\nabla\mathbf{u} + 2\left\{\hat{\mathbf{z}} + Po\left[\hat{\mathbf{s}}\sin\alpha\cos(\phi + t) - \hat{\boldsymbol{\phi}}\sin\alpha\sin(\phi + t) + \hat{\mathbf{z}}\cos\alpha\right]\right\}\times\mathbf{u} + \nabla p$$
$$= Ek\,\nabla^2\mathbf{u} - 2\hat{\mathbf{z}}s\,Po\sin\alpha\cos(\phi + t), \tag{1}$$

$$\nabla\cdot\mathbf{u} = 0, \tag{2}$$

where $\mathbf{u}$ is the velocity of fluid motion, p is the reduced pressure and the last term on the right-hand side of (1) is known as the Poincaré forcing which drives precessional flows against viscous dissipation.

In the mantle frame of reference, the flow on the bounding surface of a precessing circular cylinder is at rest, imposing that

$$\hat{\mathbf{z}}\cdot\mathbf{u} = 0 \ \text{ and } \ \hat{\mathbf{z}}\times\mathbf{u} = \mathbf{0} \tag{3}$$

on the bottom at $z = 0$ and the top at $z = 1$, and

$$\hat{\mathbf{s}}\cdot\mathbf{u} = 0 \ \text{ and } \ \hat{\mathbf{s}}\times\mathbf{u} = \mathbf{0} \ \text{ at the sidewall } \ s = \Gamma. \tag{4}$$

The strongly precessing problem defined by (1) and (2) subject to the boundary conditions (3) and (4) with $(Po\sin\alpha/\sqrt{Ek}) \ge \mathrm{O}(10)$ for $Ek \ll 1$ will be solved by a new finite element code, revealing an unusual form of the nonlinear resonant mode in a strongly precessing cylinder.

Our focus will be placed on a cylinder whose radius-height aspect ratio is $\Gamma = 0.502559$. At this aspect ratio, the precessional forcing resonates directly with the lowest-order inertial mode and, consequently, the amplitude $|\mathbf{u}|$ of the resulting flow obeys the asymptotic scaling $|\mathbf{u}| = \mathrm{O}(Po\sin\alpha/\sqrt{Ek})$ at $Ek \ll 1$ for a weakly precessing cylinder.

Prior to discussing the wall-localized mode of strongly precessing flow, it is desirable, for the purpose of comparison, to look at the structure of weakly precessing flow. Since a new finite element code is employed for the first time to compute strongly precessing flow in a cylinder, it is also desirable to briefly discuss how we validate the new code. For the problem of strongly precessing flow in rotating cylindrical cavities, local numerical methods like finite element methods are particularly suitable. This is because the standard spectral methods or finite-difference methods,

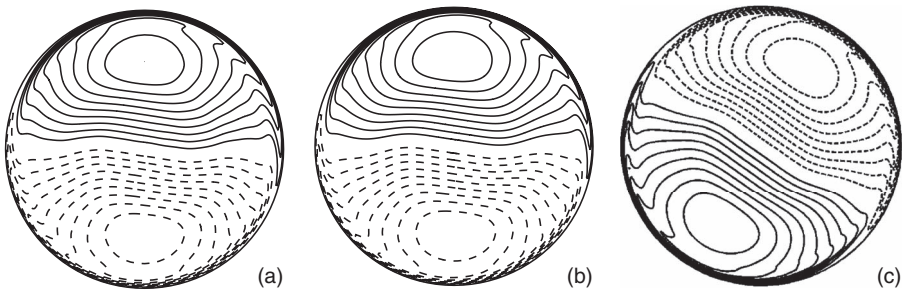

FIG. 1. Contours of the vertical velocity $\hat{\mathbf{z}} \cdot \mathbf{u}$ at the $z = 0.5$ plane of the three different solutions in a weakly precessing cylinder $\Gamma = 0.502559$ and $Ek = 10^{-4}$ obtained using three profoundly different methods: (a) the general linear asymptotic solution for $Ek \ll 1$, (b) the linear numerical solution using spectral methods, and (c) the fully nonlinear solution using the three-dimensional finite element code. Solid contours indicate $\hat{\mathbf{z}} \cdot \mathbf{u} > 0$ while dashed contours correspond to $\hat{\mathbf{z}} \cdot \mathbf{u} < 0$.

owing to the well-known axial singularities, are numerically unsuitable for nonlinear problems in cylindrical cavities. We have constructed a fully three-dimensional, nonlinear finite element model that is used to calculate strongly nonlinear flow in a precessing circular cylinder. In our finite element code, a three-dimensional tetrahedralization of the cylinder produces a finite element mesh that does not have axial singularities. Furthermore, our three-dimensional mesh is flexible enough to construct more nodes in the vicinity of the bounding surface of the cylinder for resolving the thin viscous boundary layer. In our finite element method,[11] a mixed finite element of Hood-Taylor type is adopted: in each tetrahedral element, a piecewise quadratic polynomial is employed to approximate the velocity $\mathbf{u}$ while a piecewise linear polynomial is used to approximate the pressure p. While the time step $\Delta t = 10^{-2}$ is usually adopted in the present numerical experiments, the three-dimensional mesh contains typically about 2.63×10^6 elements with the element size $h \approx 0.005$ that is capable of resolving the viscous boundary layer for $Ek \geq 5 \times 10^{-5}$. The convergence and accuracy of the numerical solutions are checked by running different numerical experiments with different Δt and different tetrahedral meshes.

Our new finite-element code is carefully validated with the asymptotic solution for $0 < Ek \ll 1$. When the cylinder is precessing slowly with $0 < Po/\sqrt{Ek} \ll 1$, the nonlinear effects are of secondary significance and the general asymptotic solution can be obtained by expanding the interior velocity and pressure in terms of the inertial modes along with the thin viscous boundary layers on the bounding surface of the cylinder.[5] The asymptotic solution describing weakly precessing flow is then derived by making an asymptotic match between the interior modes and the boundary-layer influx. For checking the asymptotic solution, the weakly precessing problem can be also solved by using a spectral method in which the velocity $\mathbf{u}$ is expanded in terms of the Chebyshev functions in the vertical and radial directions.[5] We employ both the weakly precessing solutions to validate our nonlinear finite element code when $Po/\sqrt{Ek} \ll 1$. Our direct nonlinear simulation, for instance, produces the kinetic energy of the flow $E_{\text{kin}} = 1.90 \times 10^{-7}$ for $Ek = 10^{-4}$, $Po = 10^{-4}$ with $\alpha = \pi/4$ while the general asymptotic solution yields $E_{\text{kin}} = 1.91 \times 10^{-7}$ for $Ek = 10^{-4}$, $Po = 10^{-4}$ with $\alpha = \pi/4$. As depicted in Figure 1, there also exist no noticeable differences between the weakly precessing solutions obtained using the asymptotic or spectral method, and the corresponding nonlinear finite-element solution at exactly the same parameters.

Our nonlinear finite-element code is also carefully validated with constructed exact solutions. When the cylinder is precessing strongly with $Po/\sqrt{Ek} \geq \mathrm{O}(1)$ and $0 < Ek \ll 1$, the effect of the nonlinear term $\mathbf{u} \cdot \nabla \mathbf{u}$ becomes significant and there exist no existing nonlinear asymptotic solutions that can be utilized to check the accuracy and validity of our new finite element code. An effective way of validating the code in this case is to construct an exact solution, $\mathbf{u}(s, \phi, z, t)$ and $p(s, \phi, z, t)$, that satisfies the equations

$$\frac{\partial \mathbf{u}}{\partial t} + \mathbf{u} \cdot \nabla \mathbf{u} + 2\left\{\hat{\mathbf{z}} + Po\left[\hat{\mathbf{s}} \sin\alpha \cos(\phi + t) - \hat{\boldsymbol{\phi}} \sin\alpha \sin(\phi + t) + \hat{\mathbf{z}} \cos\alpha\right]\right\} \times \mathbf{u} = -\nabla p + Ek\, \nabla^2 \mathbf{u} + \mathbf{f}(s, \phi, z, t), \tag{5}$$

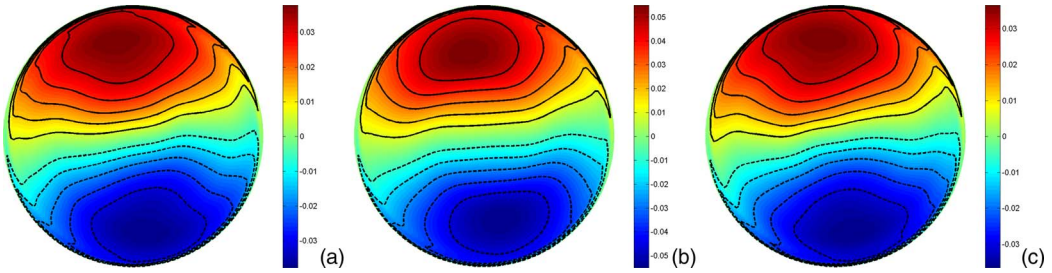

FIG. 2. Contours of the vertical velocity $\hat{\mathbf{z}} \cdot \mathbf{u}$ at three different horizonal planes: (a) at the $z = 0.75$ plane, (b) at the $z = 0.5$ plane, and (c) at the $z = 0.25$ plane for $Po = 0.005$, $\alpha = \pi/4$, and $Ek = 5 \times 10^{-5}$ with the aspect ratio $\Gamma = 0.502559$. Solid (red) contours indicate $\hat{\mathbf{z}} \cdot \mathbf{u} > 0$ while dashed (blue) contours correspond to $\hat{\mathbf{z}} \cdot \mathbf{u} < 0$.

$$\nabla \cdot \mathbf{u} = 0, \tag{6}$$

subject to the same no-slip boundary condition. Note that we have replaced the Poincaré forcing $2\hat{z}s\ Po \sin\alpha \cos(\phi + t)$ in (1) with a prescribed forcing $\mathbf{f}(s, \phi, z, t)$. An exact analytical solution to the nonlinear system (5) and (6) can be obtained by choosing an appropriate vector function $\mathbf{f}(s, \phi, z, t)$. Of course, the nonlinear system (5) and (6) are then solved using our nonlinear finite element code. We have performed various nonlinear simulations for the nonlinear system (5) and (6) at different levels of the finite element mesh, demonstrating that an excellent agreement is achieved between the nonlinear finite-element solution with a prescribed forcing $\mathbf{f}(s, \phi, z, t)$ and the constructed exact solution.

After validating our finite element code with the weakly precessing solution and the constructed exact solution, we carry out a series of numerical experiments by increasing the precession rate Po at a fixed small Ekman number at $0 < Ek \ll 1$. When $0 < Po \sin\alpha/\sqrt{Ek} \leq \mathrm{O}(1)$, the structure of the precessing flow consists of the two major components as observed in the weak precession experiments:[7] the resonant inertial mode with the amplitude $\mathrm{O}(Po \sin\alpha/\sqrt{Ek})$, which is displayed in Figure 2 for $Po = 0.005$ and $\alpha = \pi/4$ at $Ek = 5 \times 10^{-5}$ with the aspect ratio $\Gamma = 0.502559$, and the weak geostrophic mode of the order $(Po \sin\alpha/\sqrt{Ek})^2$ whose profile is typically bell-shaped with its maximum at the middle distance $s \approx 0.5\Gamma$ displayed in Figure 4(a). When the precession rate increases further to $Po \sin\alpha/\sqrt{Ek} = \mathrm{O}(10)$ at $0 < Ek \ll 1$, the structure of the weakly precessing flow becomes unstable, leading to an unusual form of the strongly precessing flow. Figure 5 shows the kinetic energy density E_{kin} of the strongly precessing flow as a function of time for $Po = 0.5$ and $\alpha = \pi/4$ at $Ek = 5 \times 10^{-5}$ with the aspect ratio $\Gamma = 0.502559$. It can be seen the kinetic energy density E_{kin} varies only slightly after the initial transient period. At the same time, the spatial structures of the strongly precessing flow also show no significant changes at different instants. In other words, the strongly precessing flow is quasi-steady with its non-axisymmetric component traveling retrogradely.

The most remarkable feature is, however, the spatial structure of the strongly precessing flow which is illustrated in Figure 3. The strongly precessing flow can be decomposed into the three major components. First, similar to the sidewall-localized convection in a rotating cylinder, the

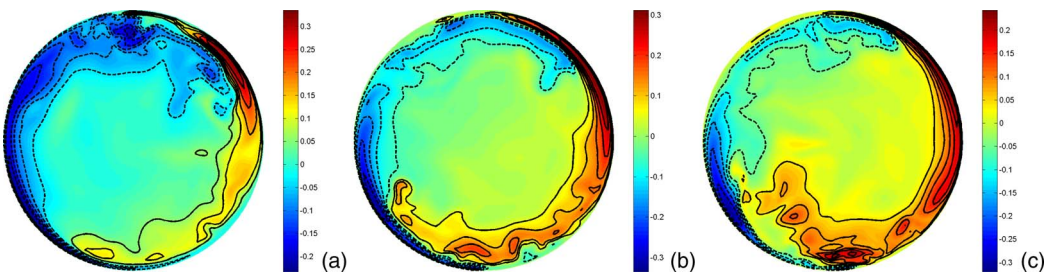

FIG. 3. Contours of the vertical velocity $\hat{\mathbf{z}} \cdot \mathbf{u}$ at three different horizonal planes: (a) at the $z = 0.75$ plane, (b) at the $z = 0.5$ plane, and (c) at the $z = 0.25$ plane for $Po = 0.5$, $\alpha = \pi/4$, and $Ek = 5 \times 10^{-5}$ with the aspect ratio $\Gamma = 0.502559$.

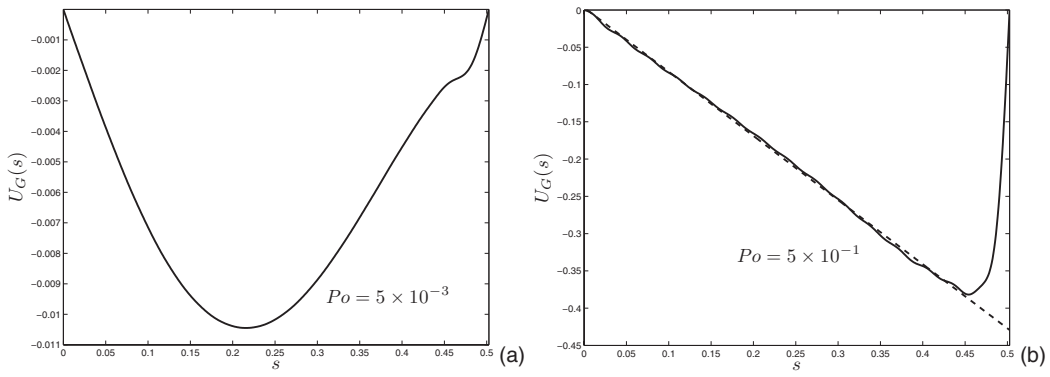

FIG. 4. (a) The geostrophic component $U_G(s)$ of the weakly precessing flow is plotted as a function of the distance s from the symmetry axis for $Po = 0.005$, $\alpha = \pi/4$, and $E = 5 \times 10^{-5}$ with the aspect ratio $\Gamma = 0.502559$. (b) The geostrophic component $U_G(s)$ (the solid line) of the strongly precessing flow is plotted as a function of s for $Po = 0.5$, $\alpha = \pi/4$, and $E = 5 \times 10^{-5}$ with $\Gamma = 0.502559$ while the dashed line represents a rigid-body rotation given by $U_G(s) = -0.86s$.

non-axisymmetric component of the flow displayed in Figure 3 is largely sidewall-localized and trapped in the vicinity of the sidewall. Second, an axisymmetric wall-localized shear is formed in the vicinity of the sidewall. Third, the strongly precessing flow in the interior of the cylinder is approximately in the form of a rigid-body rotation. The second and third components are clearly illustrated in the profile of the geostrophic component $\mathbf{U}_G$ shown in Figure 4(b) in which the geostrophic flow $U_G(s) = |\mathbf{U}_G|$ (the solid line) is plotted as a function of the distance s from the symmetry axis. Evidently, the interior geostrophic component $\mathbf{U}_G$ of the strongly precessing flow simply represents a rigid-body rotation approximately given by the formula

$$\mathbf{U}_G(s) = \Omega_G\, \hat{\mathbf{z}} \times \mathbf{r} \ \text{ in } \ 0 \le |\hat{\mathbf{z}} \times \mathbf{r}| \le (\Gamma - \delta)$$

with $\Omega_G \approx -0.86$, along with the sidewall-localized shear confined in a layer of the thickness $\delta \approx 0.05$. The direction and amplitude of the interior rigid-body rotation indicate the precession-driven flow can substantially reduce the angular momentum of the rotating fluid system. It is important to notice that the geostrophic component $\mathbf{U}_G$ is overwhelmingly predominant in the strongly precessing flow containing about 89.4% of the total kinetic energy while the directly forced inertial mode with the azimuthal wavenumber $m = 1$ contributes only about 8.59%. Furthermore, our computations indicate that both the size and amplitude of the rigid-body rotation seem to grow gradually when Po increases from $Po = 0.005$ shown in Figure 4(a) to $Po = 0.5$ in Figure 4(b).

The structure of the strongly precessing flow in the form of the sidewall-localized mode seems highly robust and stable. In order to test the stability of the sidewall-localized mode, we have run some numerical experiments sufficiently long for more than 250 rotation periods. But no instabilities are observed during the very long simulations and the structure of the sidewall-localized mode remains largely unchanged. Moreover, the nearly same sidewall-localized mode is found when the aspect ratio Γ changes slightly and when different initial conditions or different small Ekman numbers are used in the numerical experiments. It suggests that the sidewall-localized mode represents the only stable nonlinear solution in the strongly precessing regime for $Po \sin\alpha/\sqrt{Ek} = \mathrm{O}(10)$ at $0 < Ek \ll 1$ in the resonant cylinder with the aspect ratio $\Gamma \approx 0.502559$.

This letter reports an unusual form of the strongly nonlinear flow in a resonant precessing cylinder found via numerical experiments using a finite-element method. The nonlinear flow is marked by a sidewall-localized non-axisymmetric traveling wave, a wall-localized axisymmetric shear together with a dominant interior rigid-body rotation whose direction and amplitude dramatically reduce the angular momentum of the rotating fluid system. We have also performed nonlinear simulations at different values of Po, α, Ek, and Γ, indicating that the strongly nonlinear wall-localized mode is highly stable and robust, and, hence, should be identifiable in laboratory experiments. But special care is needed in order to detect the sidewall-localized mode in laboratory experiments. This is because the non-rigid-rotation fluid motion in this mode is very weak in the bulk of the cylinder and

only measurable in the vicinity of the bounding surface of the cylinder. In other words, it is perhaps experimentally difficult to measure/observe the sidewall-localized mode without having a helpful theoretical guidance.

In comparison to the sidewall-localized convection which exists only when nonlinearity is sufficiently weak, the sidewall-localized precessing flow occurs only when nonlinearity is sufficiently strong. Since the rotation axis of rotating systems in laboratory experiments is usually not parallel to the rotation axis of the Earth, the precession-driven flow would always occurs naturally in rotating fluid experiments.[12,13] It follows that understanding the dynamics and pattern of precessing flows has a wide range of implications for interpreting the observation of rotating fluid experiments.

An important question is why the sidewall-localized mode takes place in the strongly precessing cylinder and whether an asymptotic theory can be developed to describe it. It is known that the weak bell-shaped geostrophic flow in the weakly resonant cylinder shown in Figure 4(a) is induced by the weakly nonlinear Ekman boundary layers at the top and bottom ends of the cylinder[7] [see also Ref. 14]. When the precessing rate increases further, the strongly nonlinear Ekman boundary layers appear to be able to, by the same mechanism, induce and maintain the predominant geostrophic flow shown in Figure 4(b) for the strongly precessing cylinder. In a recent experimental study, Mouhali *et al.*[8] briefly mentioned that there is a loose range of precession rates where the precessing flows in the form of cyclones are found to collapse into a unique vortex occupying the whole section of the cylinder. But no details about the vortex are reported. It is likely that the vortex observed in the experiment[8] with the precession angle $\alpha = 90^\circ$ for the non-resonant aspect ratio $\Gamma = 0.427$ is in some ways related to the sidewall-localized mode discussed in this letter. It remains unclear whether the nature of the sidewall-localized shear depicted in Figure 4(b) is of the Stewartson type similar to the shear layers induced in a spherical shell by differentially rotating the inner and outer spheres[15] or is analogous with the shear layer revealed in differentially rotating spherical shells.[16] A full understanding of the sidewall-localized mode requires a nonlinear asymptotic theory for $Po \sin\alpha/\sqrt{Ek} = \mathrm{O}(10)$ at $0 < Ek \ll 1$. In contrast to the weakly precessing problem, deriving such a strongly nonlinear asymptotic solution for the sidewall-localized precessing flow represents a mathematically challenging task (Figure 5).

It was numerically demonstrated that the nonlinear flow in a precessing cylinder can trigger dynamo action[17] (see also Ref. 18). Moreover, a laboratory dynamo experiment using a precessing cylinder will be carried out at Helmholtz-Zentrum Dresden-Rossendorf in Germany. Our results suggest that the strongly nonlinear sidewall-localized flow – in which the sidewall-localized non-axisymmetric flow shown in Figure 3 would produce an α-effect while the sidewall-localized shear illustrated in Figure 4(b) would generate a strong toroidal magnetic field – would be a suitable candidate for efficient dynamo action in a precessing cylinder.

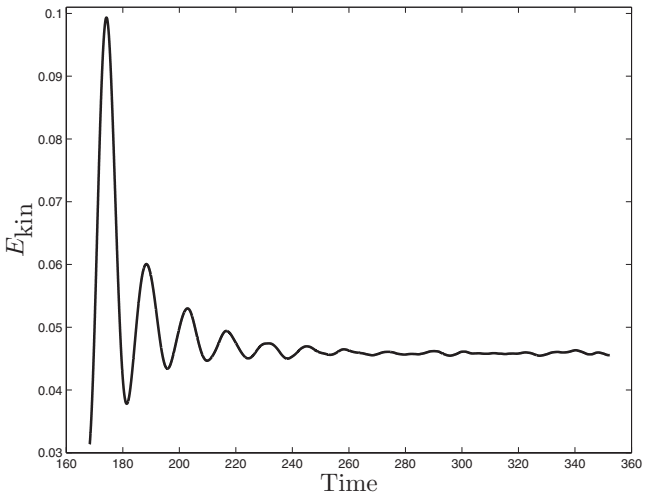

FIG. 5. Kinetic energy density, E_{kin}, of the strongly precessing flow as a function of time for $Po = 0.5$, $\alpha = \pi/4$ with $Ek = 5 \times 10^{-5}$ and the aspect ratio $\Gamma = 0.502559$.

K.Z. is grateful to A. Tilgner for helpful discussions about this paper. K.Z. is supported by grants from UK Science and Technology Facilities Council and Natural Environment Research Council. X.L. is supported by National Natural Science Foundation of China/11133004 and Chinese Academy of Sciences under Grant Nos. KZZD-EW-01-3 and XDB09000000.

[1] H. F. Goldstein, E. Knobloch, I. Mercader, and M. Net, "Convection in a rotating cylinder. Part 1. Linear theory for moderate Prandtl numbers," J. Fluid Mech. **248**, 583–604 (1993).
[2] J. Herrmann and F. H. Busse, "Asymptotic theory of wall-localized convection in a rotating fluid layer," J. Fluid Mech. **255**, 183–194 (1993).
[3] X. Liao, K. Zhang, and Y. Chang, "On boundary-layer convection in a rotating fluid layer," J. Fluid Mech. **549**, 375–384 (2006).
[4] K. Zhang and X. Liao, "The onset of convection in rotating circular cylinders with experimental boundary conditions," J. Fluid Mech. **622**, 63–73 (2009).
[5] X. Liao and K. Zhang, "On flow in weakly precessing cylinders: The general asymptotic solution," J. Fluid Mech. **709**, 610–621 (2012).
[6] R. Manasseh, "Breakdown regimes of inertia waves in a precessing cylinder," J. Fluid Mech. **243**, 261–296 (1992).
[7] P. Meunier, C. Eloy, R. Lagrange, and F. Nadal, "A rotating fluid cylinder subject to weak precession," J. Fluid Mech. **599**, 405–440 (2008).
[8] W. Mouhali, T. Lehner, J. Leorat, and R. Vitry, "Evidence for a cyclonic regime in a precessing cylindrical container," Exp. Fluids **53**, 1693–1700 (2012).
[9] J. J. Kobine, "Azimuthal flow associated with inertial wave resonance in a precessing cylinder," J. Fluid Mech. **319**, 387–406 (1996).
[10] R. F. Gans, "On the precession of a resonant cylinder," J. Fluid Mech. **41**, 865–872 (1970).
[11] K. Chan, K. Zhang, and X. Liao, "An EBE finite element method for simulating nonlinear flows in rotating spheroidal cavities," Int. J. Numer. Meth. Fluid **63**, 395–414 (2010).
[12] J. Boisson, D. C. Cébron, F. Moisy, and P.-P. Cortet, "Earth rotation prevents exact solid-body rotation of fluids in the laboratory," Europhys. Lett. **98**, 59002 (2012).
[13] S. A. Triana, D. S. Zimmerman, and D. P. Lathrop, "Precessional states in a laboratory model of the Earth's core," J. Geophys. Res. **117**, B04103, doi:10.1029/2011JB009014 (2012).
[14] F. H. Busse, "Steady fluid flow in a precessing spheroidal shell," J. Fluid Mech. **33**, 739–751 (1968).
[15] R. Hollerbach, "Instabilities of the Stewartson layer. Part 1. The dependence on the sign of Ro," J. Fluid Mech. **492**, 289–302 (2003).
[16] C. Baruteau and M. Rieutord, "Inertial waves in a differentially rotating spherical shell," J. Fluid Mech. **719**, 47–81 (2012).
[17] C. Nore, J. Leorat, J.-L. Guermond, and F. Luddens, "Nonlinear dynamo action in a precessing cylindrical container," Phys. Rev. E **84**, 016317 (2011).
[18] A. Tilgner, "Precession driven dynamos," Phys. Fluids **17**, 034104–034106 (2005).